


Histidine methyltransferase SETD3 methylates structurally diverse histidine mimics in actin

Jordi C. J. Hintzen¹ | Huida Ma² | Hao Deng³ | Apolonia Witecka⁴ |
 Steffen B. Andersen¹ | Jakub Drozak⁴ | Hong Guo^{5,6} | Ping Qian³ |
 Haitao Li² | Jasmin Mecinović¹ 

¹Department of Physics, Chemistry and Pharmacy, University of Southern Denmark, Odense, Denmark

²MOE Key Laboratory of Protein Sciences, Beijing Frontier Research Center for Biological Structure, School of Medicine, Tsinghua-Peking Center for Life Sciences, Tsinghua University, Beijing, China

³Chemistry and Materials Science Faculty, Shandong Agricultural University, Tai'an, Shandong, China

⁴Department of Metabolic Regulation, Faculty of Biology, University of Warsaw, Warsaw, Poland

⁵Department of Biochemistry and Cellular and Molecular Biology, University of Tennessee, Knoxville, Tennessee, USA

⁶UT/ORNL Center for Molecular Biophysics, Oak Ridge National Laboratory, Oak Ridge, Tennessee, USA

Correspondence

Ping Qian, Chemistry and Materials Science Faculty, Shandong Agricultural University, Tai'an, China.
 Email: qianp@sdau.edu.cn

Haitao Li, MOE Key Laboratory of Protein Sciences, Beijing Frontier Research Center for Biological Structure, School of Medicine, Tsinghua-Peking Center for Life Sciences, Tsinghua University, Beijing 100084, China.
 Email: lht@tsinghua.edu.cn

Jasmin Mecinović, Department of Physics, Chemistry and Pharmacy, University of Southern Denmark, Campusvej 55, 5230 Odense, Denmark.
 Email: mecinovic@sdu.dk

Funding information

H2020 European Research Council, Grant/Award Number: 715691; Narodowe Centrum Nauki, Grant/Award Number: 2017/27/B/NZ1/00161; National Natural Science Foundation of China, Grant/Award Numbers: 22177064, 31725014; Natural Science Foundation of Shandong Province, Grant/Award Number: ZR2021MB050; National Key Research Development Program of China, Grant/Award Number: 2020YFA0803300

Review Editor: John Kuriyan

Abstract

Actin histidine N^ε-methylation by histidine methyltransferase SETD3 plays an important role in human biology and diseases. Here, we report integrated synthetic, biocatalytic, biostructural, and computational analyses on human SETD3-catalyzed methylation of actin peptides possessing histidine and its structurally and chemically diverse mimics. Our enzyme assays supported by biostructural analyses demonstrate that SETD3 has a broader substrate scope beyond histidine, including N-nucleophiles on the aromatic and aliphatic side chains. Quantum mechanical/molecular mechanical molecular dynamics and free-energy simulations provide insight into binding geometries and the free energy barrier for the enzymatic methyl transfer to histidine mimics, further supporting experimental data that histidine is the superior SETD3 substrate over its analogs. This work demonstrates that human SETD3 has a potential to catalyze efficient methylation of several histidine mimics, overall providing mechanistic, biocatalytic, and functional insight into actin histidine methylation by SETD3.

KEYWORDS

biocatalysis, histidine, methylation, SETD3, β -actin

Jordi C. J. Hintzen, Huida Ma, and Hao Deng contributed equally to this study.

This is an open access article under the terms of the Creative Commons Attribution-NonCommercial License, which permits use, distribution and reproduction in any medium, provided the original work is properly cited and is not used for commercial purposes.

© 2022 The Authors. *Protein Science* published by Wiley Periodicals LLC on behalf of The Protein Society.

1 | INTRODUCTION

Actin is an essential constituent of microfilaments that form the cytoskeleton of eukaryotic cells, and thus plays an important role in maintaining the structure of the cell.^{1–4} Human actin exists in six isoforms that show different cellular expression patterns and functions.⁵ Among these six isoforms, β -actin (β A) is expressed ubiquitously in the cell and plays the central role in cytoskeletal stability and cell mobility.⁶ Actin exists freely in the cell as a monomeric globular protein (G-actin), which upon binding to ATP polymerizes and forms stable actin filaments (F-actin).⁷ These filaments represent a crucial part of the cellular architecture, and their length is controlled by hydrolysis of the terminal phosphate of bound ATP, which is released slowly and leads to depolymerization of the filament.^{8,9} To fine-tune their physiological roles, many posttranslational modifications (PTMs)—including methylation, acetylation, SUMOylation, and ubiquitination—have been found on actin proteins.¹⁰ N^τ -methylation of the histidine residue at position 73 in β A (β A-His73) has been shown to be conserved among eukaryotic actin isoforms, and leads to a decreased rate of hydrolysis of the actin-bound ATP.^{11,12} Histidine methylation prevents primary dystocia and plays a key role in parturition in female mice.¹³ SETD3 was recently identified as the actin-specific histidine methyltransferase that in the presence of the S-adenosylmethionine (SAM) cosubstrate catalyzes N^τ -methylation of His73 in β A (Figure 1a).^{13–15} SETD3 is a member of the SET-domain containing methyltransferases, a large family of enzymes that catalyze methylation of lysine and arginine residues on histones and non-histone proteins.¹⁶ The SET-domain is an \sim 130 amino acids long motif, which stands for Su(var)3–9, Enhancer of zeste, and Trithorax.¹⁷ Initially, SETD3 was identified as a histone lysine methyltransferase that catalyzes monomethylation and dimethylation of histone H3 at positions K4 and K36,^{18,19} however, a H3 peptide was shown to be a very poor substrate for SETD3 in comparison to a β A peptide fragment.²⁰

As the imidazole ring of histidine contains two nitrogen atoms at the N^π and N^τ position (it is noteworthy that there has been often a confusion in the literature about the numbering of N atoms in histidine, as they are also called N^1 and N^3 , respectively; to avoid confusion we prefer the N^π and N^τ nomenclature) (Figure 1a), SETD3 could in principle have an ability to catalyze methylation of either or even both of these nitrogens. X-ray crystallographic and biochemical studies have shown, however, that SETD3 specifically catalyzes the methylation of histidine at the N^τ position, that is, a more distant nitrogen atom at the histidine side chain (Figure 1a).^{13,20–22}

Structural analyses of ternary complexes revealed that the β A peptide lies in a narrow groove formed by the SET domain of SETD3, with the imidazole ring of His73 buried in a hydrophobic pocket (Figure 1b). In the crystal structures containing the unmethylated His73 and S-adenosylhomocysteine (SAH; Figure 1b), N^τ of His73 in the β A peptide donates a hydrogen bond to the backbone carbonyl group of Asp275 and therefore exists as the N^τ -H tautomeric form that cannot undergo the methylation. Two different mechanisms seem to be possible. One is that there would be some general acid/base catalyst(s) that convert the N^τ -H tautomer to the N^π -H tautomer for methylation.^{20,21,23} Nevertheless, such general acid/base catalysts have not been identified with clarity, and replacement of some potential residues at the active site, for instance Asn255 by Ala or Tyr312 by Phe, did not abolish the enzyme's activity. Alternatively, it was proposed that His73 in the N^π -H tautomeric form may bind to SETD3 directly for methylation.²³ This suggestion seems to be consistent with several of the available crystal structures for actin,^{24,25} which show that the N^π atom of His73 (or from N^τ -Me-His73 after the methylation on N^τ) donates a hydrogen bond to the backbone carbonyl oxygen of Gly158, indicating His73 of actin may exist as the N^π -H tautomer. In either of the two mechanisms, the chemical process of methylation is expected to start from the SETD3, N^π -H tautomer complex. Computer

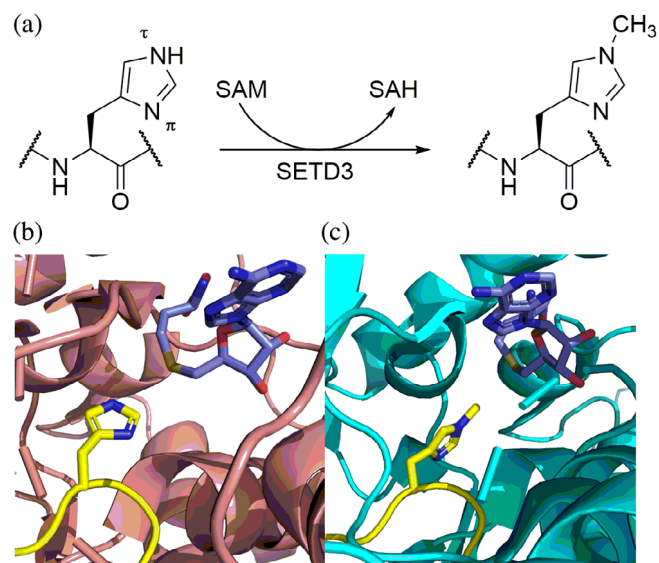


FIGURE 1 (a) SETD3-catalyzed N^τ -methylation of histidine in β A. (b) View from a crystal structure of SETD3 (pink) complexed with an unmodified β A peptide (yellow) and SAH, an unreactive product of the methylation reaction (blue; PDB ID: 6ICV). (c) View from a crystal structure of SETD3 (cyan) complexed with a N^τ -methylated β A peptide (yellow) and SAH (blue; PDB ID: 6ICT)

simulations demonstrated that the N^{π} -H tautomer was stable and well positioned and could undergo methylation at the SETD3 active site.²³ Interestingly, the imidazole ring of the N^{π} -H tautomer from the simulations was found to have an orientation that is similar to the one in the crystal structures of the product complex containing N^{τ} -Me-His73 (Figure 1c), suggesting that the imidazole ring might not undergo rotation during the methylation reaction.

Recent biochemical and biostructural studies have revealed that SETD3 exhibits a selectivity for histidine over lysine and methionine.^{20,21,26,27} The histidine-binding pocket appears to be too small to efficiently accommodate the longer aliphatic side chain of lysine, although lysine's side chain could be traced around the outer part of histidine's imidazole ring, leading to the lysine's terminal amine positioned alike the N^{τ} of histidine's imidazole. However, it was found that a crucial tyrosine residue, which forms cation- π interactions with lysine in SET domain-containing histone lysine methyltransferases,²⁸ is not present in SETD3 where it is replaced by asparagine (Asn255) that seems to play an essential role in substrate binding and histidine methylation, forming a stabilizing hydrogen bond with the N^{π} -H tautomer of histidine²³ or the methylated histidine in product. Further cementing SETD3 as a histidine specific methyltransferase, an engineered SETD3 was generated wherein Asn255 was replaced by Phe, as well as Trp273 substituted by Ala to allow for more physical space for Lys's side chain and to prevent steric clash in the hydrophobic binding pocket; these modifications caused SETD3 to display a 13-fold preference for lysine over

histidine in a β A peptide.²⁷ Flanking the His73 binding site is the secondary Ile71 pocket that binds structurally diverse hydrophobic side chains.²⁹ Furthermore, SETD3 was also shown to have an ability to poorly methylate methionine, generating *S*-methylmethionine.²⁶ Interestingly, the methionine-containing β A peptide has a 76-fold stronger binding affinity and efficiently inhibits the activity of SETD3.²⁶ β A peptides possessing methionine analogs at the His73 position were shown to inhibit SETD3 with nanomolar potency.³⁰ Owing to SETD3's unique reactivity toward histidine over lysine and methionine, we sought to explore the substrate specificity of SETD3 to gain a deeper understanding of the underlying mechanism and biocatalytic scope of the SETD3 histidine methyltransferase. Here, we report biomolecular studies on human SETD3-catalyzed methylation of histidine and its simplest mimics incorporated into β A peptides. Our synergistic synthetic, enzymatic, biostructural, and computational work demonstrates that SETD3 has a broader substrate specificity beyond histidine.

2 | RESULTS AND DISCUSSION

2.1 | The panel of histidine analogs

To investigate SETD3's unique ability to catalyze an efficient methylation of histidine, we set out to incorporate a structurally and chemically diverse panel of histidine analogs into the β A peptide and examine the substrate scope of the human SETD3-catalyzed methylation reactions of β A (Figure 2). We have designed a large panel of

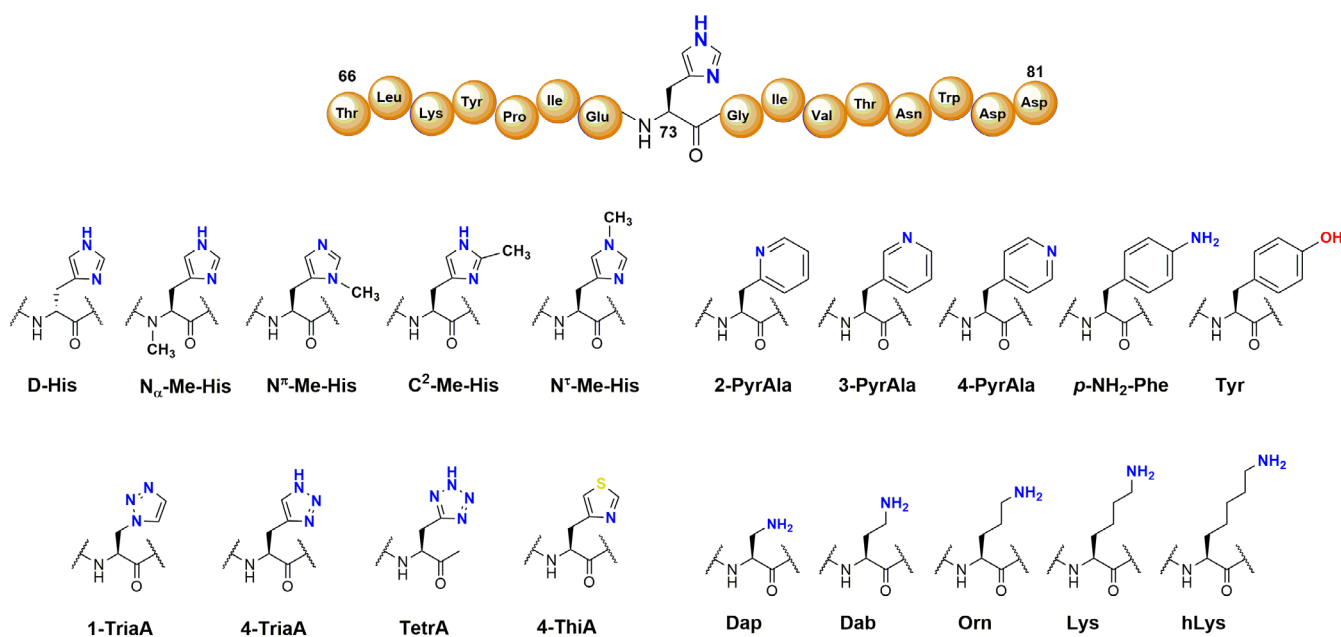


FIGURE 2 The panel of histidine analogs incorporated in the β A peptide for examination of SETD3 catalysis

histidine analogs that cover a wide chemical space, thus advancing basic understanding of SETD3 catalysis and its biocatalytic potential. The following histidine analogs have been selected: (i) D-histidine to probe the stereochemistry; (ii) N α -methylhistidine to explore the importance of the backbone; (iii) premethylated N $^{\pi}$ -methylhistidine and N $^{\tau}$ -methyl-histidine to further confirm the site of methylation; (iv) C 2 -methyl-histidine to probe for steric effect on the imidazole ring; (v) two triazolylalanines and the tetrazolylalanine to probe the most subtle change in reactivity of the imidazole ring; (vi) pyridylalanines and *para*-amino phenylalanine to investigate both the steric effects of a six-membered ring and the subtle change in the nitrogen's location in the catalytic pocket of SETD3; (vii) 3-(4-thiazolyl)alanine and tyrosine to explore methylation of sulfur or oxygen nucleophiles, respectively, and (viii) lysine analogs to establish the optimal side chain length for SETD3-catalyzed methylation of aliphatic amines. All histidine analogs were incorporated at position 73 of the synthetic β A peptide (16-mer, residues 66–81) using automated, microwave assisted solid-phase peptide synthesis (SPPS). Coupling of the Fmoc-protected histidine analogs went smoothly, with no indicative change in reactivity observed in comparison to L-histidine. After cleavage from the Rink-Amide resin with TFA, all synthetic β A peptides were purified by reverse phase HPLC and lyophilized (Table S1 and Figures S1–S20).

To synthesize the triazol-1-yl-alanine, azidoalanine (Aza) was incorporated into the β A peptide directly (Figure S21a). After cleavage from the resin and purification, a biorthogonal copper-catalyzed click reaction enabled the preparation of the target triazole.³¹ To this end, TMS-acetylene was used, after which the TMS protecting group was removed under acidic conditions to generate the triazol-1-yl-alanine. The triazol-4-yl-alanine was generated by introduction of propargylglycine into the β A peptide and the click reaction was performed using sodium azide, affording the target triazole directly (Figure S21b). C 2 -methyl histidine was generated directly by employing a late-stage functionalization of the histidine-containing β A peptide, using sodium methanesulfinate in the presence of tert-butylhydroperoxide (TBHP) as the oxidant (Figure S21c).³²

2.2 | SETD3-catalyzed methylation by MALDI-TOF MS

We carried out enzymatic assays with the synthetic 16-mer β A peptides using MALDI-TOF MS assays.³⁰ A β A peptide (10 μ M) was incubated in the presence of the recombinantly expressed human SETD3 (1 μ M) and SAM cosubstrate (100 μ M) at 37°C (standard conditions). All

peptides possessing histidine and its analogs were studied at pH 7.2, pH 9.0, and pH 10.5; enzymatic mixtures were quenched after 1 and 3 hr. Under these conditions, the histidine-containing β A-His73 peptide was quantitatively monomethylated in 1 hr at all three pHs, without producing any dimethylated histidine (Figure 3a and Figure S22 and S23). Control reactions in the absence of either the SAM cosubstrate or the SETD3 enzyme afforded no detectable methylation of the peptide, indicating that methylation reactions are enzymatic and require the SAM cosubstrate (Figure S24). In contrast, D-histidine-containing β A-D-His73 was not shown to be methylated by SETD3 within detection limits, demonstrating that the stereochemistry of histidine is an important molecular requirement of the substrate methylation (Figure 3b and Figures S22 and S23). These data are in line with a general lack of enzymatic methylation of D-lysine residues in histones by SET domain histone lysine methyltransferases (KMTs).³³ Under standard conditions, N α -Me-histidine also did not undergo SETD3-catalyzed methylation (Figure 3c and Figures S22 and S23). We attribute the lack of observed methylation to disruption of an essential H-bond between His73's main chain amide NH and the Tyr312's main chain CO in SETD3 that likely contributes to the correct positioning of the His73 side chain for efficient methylation reaction. These results resemble data from enzymatic studies that showed the importance of the lysine's backbone for efficient KMT-catalyzed methylation reaction.³⁴

Interestingly, our MALDI-MS data showed that SETD3 has the ability to catalyze methylation of the premethylated N $^{\pi}$ -Me-His, producing N $^{\pi}$,N $^{\tau}$ -dimethylhistidine. Previous studies have shown that SETD3 specifically catalyzes methylation at the N $^{\tau}$ -position,²⁰ and under our assay conditions trace amounts of dimethylated histidine were found when using the β A-N $^{\pi}$ -Me-His73 substrate at pH 7.2 and 10.5 after 3 hr (Figures S22 and S23), and 44% of dimethylated product at pH 9.0 after 3 hr (Figure 3d). β A-C 2 -Me-His73 (Figure 3e and Figures S22 and S23) also underwent SETD3-catalyzed methylation, generating the C 2 ,N $^{\tau}$ -dimethylhistidine. In contrast, β A-N $^{\tau}$ -Me-His73 did not undergo SETD3-catalyzed methylation under standard conditions (Figure 3f and Figures S22 and S23), further cementing SETD3 as a N $^{\tau}$ -specific histidine methyltransferase.

β A-1-TriaA73 underwent SETD3-catalyzed methylation to a minor extent after 3 h at pH 7.2 (Figure S22), while no methylation was observed at pH 9.0 and 10.5 (Figure 3g and Figure S23). Notably, β A-4-TriaA73 was found to be fully methylated after 3 hr at pH 7.2 and pH 9.0 (Figure 3h and Figure S22), displaying similarity with the β A-His73 peptide at physiological and slightly basic pH values. At pH 10.5, β A-4-TriaA73 was methylated only to a minor extent (Figure S23). This observation

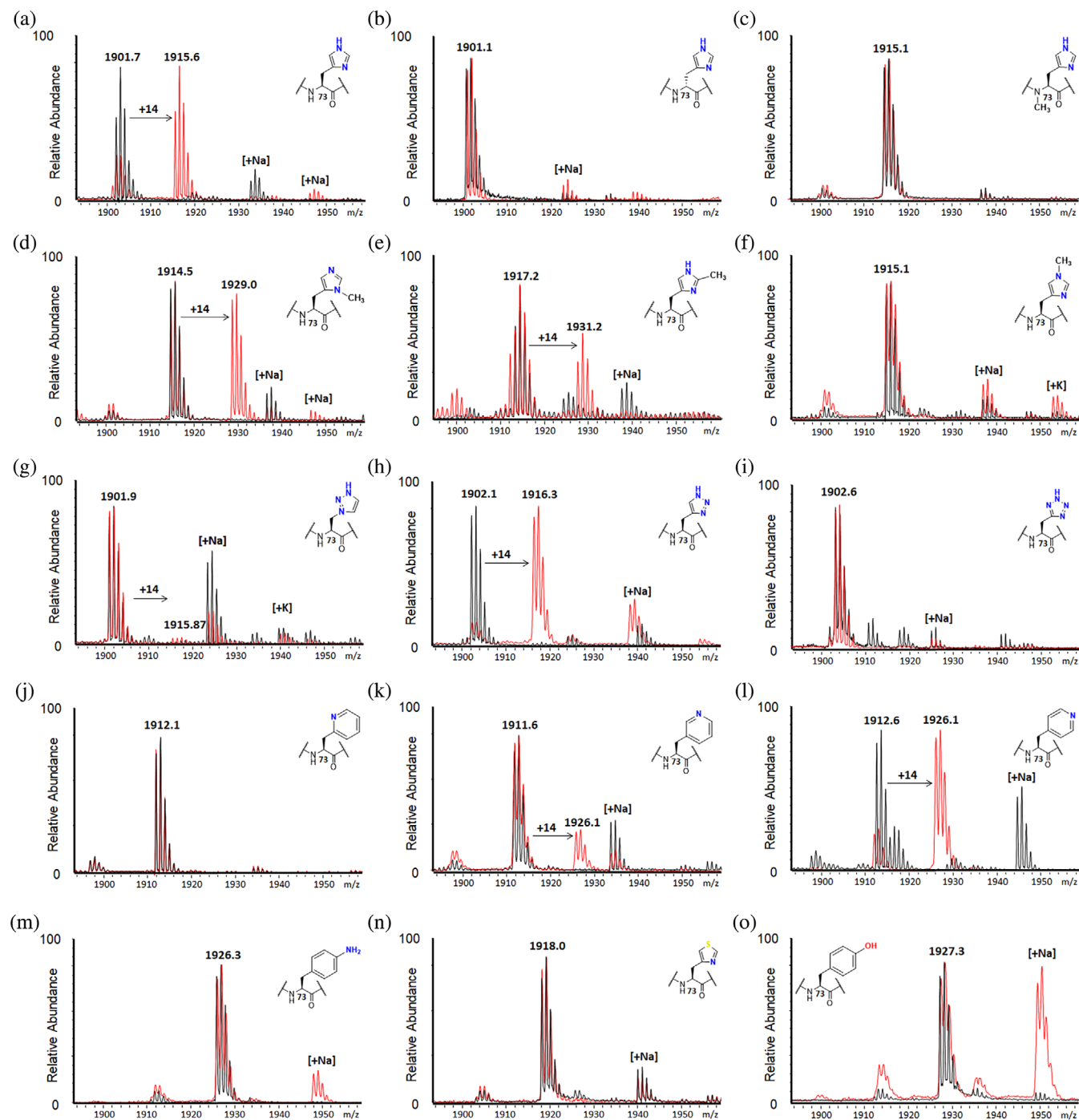


FIGURE 3 MALDI-TOF MS data showing methylation of βA_{66-81} peptides (10 μM) in presence of SETD3 (1 μM) and SAM (100 μM) after 3 hr at pH 9.0. Control reactions without SETD3 present are shown in black, SETD3-catalyzed reactions are shown in red. (a) βA -His73. (b) βA -D-His73. (c) βA - N_{α} -Me-His73. (d) βA - N_{ϵ} -Me-His73. (e) βA -C²-Me-His73. (f) βA - N_{ϵ} -Me-His73. (g) βA -1-TriaA73. (h) βA -4-TriaA73. (i) βA -TetraA73. (j) βA -2PyrAla73. (k) βA -3PyrAla73. (l) βA -4PyrAla73. (m) βA -*p*-NH₂-Phe73. (n) βA -4ThiA73. (o) βA -Tyr73

could be attributed to the difference in pK_a values between the imidazole (14.4) and the triazole (9.3), causing the triazole to be predominantly deprotonated at pH 10.5.³⁵ As the triazol-1-yl-alanine does not contain a free hydrogen on a nitrogen atom in the imidazole ring, and the triazol-4-yl-alanine does, these results indicate

that this hydrogen atom appears to be important for enzymatic activity through the hydrogen bonding stabilization of the ring configuration as observed in the case of βA -His73 (see below). Finally, βA -TetraA73 was not methylated beyond the detection limits at all three pHs (Figure 3i and Figures S22 and S23). Due to low pK_a

value of tetrazole (4.9), making it a well-known carboxylic acid bioisostere, the tetrazole side chain should be fully deprotonated at pH 7.2, likely leading to nonoptimal binding and the lack of methylation. At lower pH values (3.5 and 5.0), β A-TetrA73 underwent minor methylation in the presence of 1 μ M SETD3 (Figure S25) and significant methylation in the presence of 10 μ M SETD3 (Figure S26), unlike β A-His73 and β A-4-TriaA73 peptides. It has to be noted that all these reactions did not progress between 1 and 3 hr timepoints, indicating that the enzyme itself indeed becomes inactive at low pH (Figure S27). Taken together, these findings seem to support that the electronic properties of the nitrogen-containing aromatic ring are crucial, and that the activity of SETD3 can be fine-tuned across a range of pH values to specifically methylate certain groups.

Of the more sterically demanding six membered rings, none of the pyridylalanine-containing peptides was methylated by SETD3 at pH 7.2 (Figure S22), while strikingly, 3- and 4-pyridylalanine underwent an efficient SETD3-catalyzed methylation at pH 9.0 (Figure 3k,l). Under standard conditions, β A-4PyrAla73 reached 80% conversion after 3 hr, while β A-3PyrAla73 was methylated less efficiently, reaching 20% methylation. At pH 10.5, methylation activity for β A-3PyrAla73 was completely abolished, while β A-4PyrAla73 was still accepted as a substrate relatively well (21% conversion, Figure S24). β A-2PyrAla73, or an exocyclic amino group in β A-*p*-NH₂-Phe73, was not methylated by SETD3 at all three-tested pHs (Figure 3j,m and Figures S23 and S24). These results suggest that SETD3 is very sensitive to the positioning of the nitrogen atom to be methylated. The orientation in the 4-pyridyl is closest to the original N^r of the imidazole ring of His, while the orientation of the 2-pyridyl would line up most with the N^x nitrogen of the imidazole, leaving the 3-pyridyl positioned in between the two imidazole nitrogens. SETD3 thus clearly shows a preference for the 4-pyridyl orientation over the 3-pyridyl. Intrigued by the fact that the β A-3PyrAla73 and β A-4PyrAla73 peptides were accepted to a lesser extent at pH 10.5 in comparison to pH 9.0, we investigated whether the methylated product of the reaction is stable under more basic conditions. This revealed that only after 1 hr at pH 10.5, all the methylated 3-pyridyl analog was degraded to 3-pyridylalanine (Figure S28), confirming the finding that no methylation was observed after incubation in reaction buffer with SETD3 at pH 10.5.

Our further examinations revealed that SETD3 catalysis appears to be limited to nitrogen nucleophiles within the scope of our panel. The 4-thiazolyl-alanine containing peptide was not methylated, indicating that SETD3 is not

capable of methylation of sulfur in an aromatic system, even though it is at the same position as the N^r of histidine (Figure 3n and Figures S22 and S23). Incorporation of tyrosine did not lead to methylation (Figure 3o and Figures S22 and S23), which could be due to several reasons, including the steric demand of the six membered ring, the existence of an oxygen nucleophile instead of nitrogen, and the target group lying outside of the ring, which was not methylated in the case of an amino group either.

To further investigate the effect of lysine's aliphatic side chain on the efficiency of the SETD3-catalyzed methylation, β A peptides bearing diaminopropionic acid (Dap), diaminobutyric acid (Dab), ornithine (Orn), lysine (Lys), and homolysine (hLys) were examined under the same assay conditions as described above. In principle, SETD3 might have an ability of catalyzing three subsequent methylation steps on the terminal amino group of the Lys and its analogs, much alike other KMTs. Our results revealed that at pH 7.2 none of the Lys analogs was methylated (Figure S22), while at pH 9.0 methylation was only observed for Dab and Orn to a minor extent (Figure S29). At pH 10.5, however, only minor monomethylation of Dab and Orn was observed (Figure S23). These results indicate that Dab and Orn have chain lengths that are better accommodated by the smaller active site of SETD3, in comparison to SET-domain Lys methyltransferases. However, as previously described,²¹ the Lys containing β A-Lys73 is a much poorer substrate than the histidine containing β A-His73, therefore higher concentrations of enzyme for the panel were used to assess which of Lys analogs possesses the optimal chain length. Lys analog-containing β A peptides (10 μ M) were incubated in the presence of human SETD3 (10 μ M) and SAM cosubstrate (200 μ M) at 37°C (Figure 4). Interestingly, only minor monomethylation for Dab (7%) and Orn (14%) was observed already at pH 7.2 after 3 hr, with no Lys methylation observed (Figure S30). At pH 9.0, only Dab, Orn, and Lys showed monomethylation, with some dimethylation also observed for Orn (Figure S31). At pH 10.5, similar profiles as at pH 9.0 were observed for Dab and Lys (Figure 4b,d), however, Orn now showed the major part of the starting material converted, and monomethylation, dimethylation, and trimethylation were readily observed at 35, 32, and 6%, respectively (Figure 4c). Dap and hLys were not found to be methylated under any of the pHs, even in the presence of an increased concentration of SETD3 (Figure 4a,e and Figures S30 and S31). A consumption curve with β A-Orn73 showed a gradual decrease of the unmethylated β A-Orn73 and a sequential increase of methylated species in a period of 3 hr (Figure 4f).

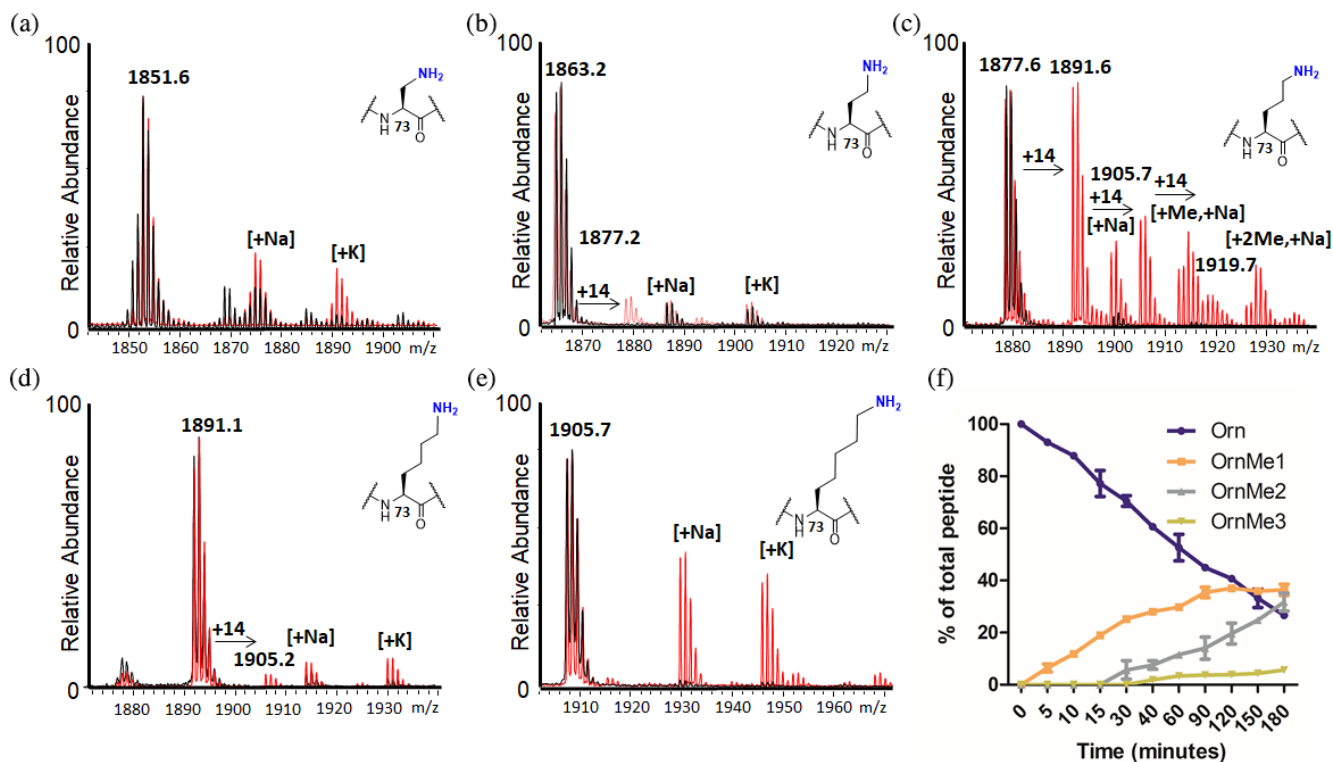


FIGURE 4 MALDI-TOF MS data showing methylation of β A peptides (10 μ M) possessing Lys analogs in presence of increased concentration of SETD3 (10 μ M) and SAM (200 μ M) after 3 h at pH 10.5. Control reactions without SETD3 present are shown in black, SETD3-catalyzed reactions shown in red. (a) β A-Dap73. (b) β A-Dab73. (c) β A-Orn73. (d) β A-Lys73. (e) β A-hLys73. (f) Consumption curve of the SETD3-catalyzed methylation of β A-Orn73 at pH 10.5

2.3 | Enzyme kinetics for SETD3-catalyzed methylation of histidine analogs

Having established that some histidine analogs can be accepted for SETD3-catalyzed methylation, we sought to investigate their kinetic profiles. MALDI-TOF MS kinetic studies were used under steady-state conditions varying the concentration of the synthetic β A peptides in the kinetic buffer at pH 9.0. The concentration of SETD3 was adjusted to accommodate linear conversion for the analogs in a time window of 20 min at 37°C. Out of our tested β A peptides, the β A-His73 substrate still had the best catalytic efficiency (k_{cat}/K_m , Table 1 and Figure S32a), while β A-4PyrAla73 and β A-4-TriaA73 displayed threefold and twofold decrease in the catalytic efficiency, respectively (Table 1 and Figures S32c and S32e). Interestingly, the catalytic rate k_{cat} for the 4-TriaA is—within the margin of error—the same as for the natural substrate, the loss in activity here is caused by an apparent loss of binding, as reflected by a higher K_m value. On the other hand, it was found that β A-4PyrAla73 and β A-His73 display similar K_m values, and the decrease in activity for β A-4PyrAla73 is attributed to a less favorable k_{cat} . These two histidine analogs appeared to be the best substrates within our panel, while the two other

tested analogs, β A-N^T-Me-His73 and β A-3PyrAla73, displayed a significantly lower catalytic efficiency (12- and sixfold) in comparison to β A-His73 (Table 1 and Figures S32b and S32d). For β A-Orn73 a 25-fold reduced substrate efficiency was observed, however, it was tested at pH 9.0 for direct comparison with other analogs; whereas, it was shown to be better accommodated at pH 10.5 (Figure S32f). As suggested from data in Figure 4, and comparing to previously reported results for Lys²¹ with the SETD3, Orn appears to be a much better substrate than Lys, owing to the fact that Orn is a better histidine mimic and its side chain can be better positioned into the catalytic pocket of SETD3 for efficient methylation reaction.

Next, we tested the analogs that were not accepted for SETD3-catalyzed methylation for their potency as inhibitors of SETD3. Due to difficulties with overlapping signals in our mass spectrometric assay, β A-N_α-Me-His73, β A-N^T-Me-His73, β A-1-TriaA73, and β A-Tetra73 were omitted from the panel, whereas analogs that were not methylated were tested in a single-point screening assay. SETD3 (180 nM) was incubated for 1 hr at pH 9.0 with the potential inhibitory peptides (100 μ M) and SAM (100 μ M), subsequently the β A-His73 peptide (10 μ M) was added and reacted for 20 min to ensure linear

Peptide	k_{cat} (min^{-1})	K_{m} (μM)	$k_{\text{cat}}/K_{\text{m}}$ ($\mu\text{M}^{-1} \text{min}^{-1}$)
$\beta\text{A-His73}$	141 ± 7.4	33.6 ± 4.7	4.22
$\beta\text{A-N}^{\tau}\text{-me-His73}$	28.2 ± 2.5	88.6 ± 16	0.32
$\beta\text{A-4-TriaA73}$	138 ± 9.6	66.7 ± 11	2.07
$\beta\text{A-3PyrAla73}$	48.8 ± 3.0	62.9 ± 9.1	0.78
$\beta\text{A-4PyrAla73}$	47.6 ± 4.4	33.8 ± 8.3	1.41
$\beta\text{A-Orn73}$	14.0 ± 1.2	95.8 ± 16	0.15

TABLE 1 Kinetic parameters for SETD3-catalyzed methylation of βA peptides

conversion to the methylated species. All analogs containing an aromatic ring-structure in the side chain, along with the Lys analogs Dap and hLys were found to be inactive, with apparent IC_{50} values above $100 \mu\text{M}$ (Figure S33).

2.4 | Calorimetric titration studies of SETD3 with analog βA peptides

To explore the substrate specificity of SETD3, we measured the binding affinities by isothermal titration calorimetry (ITC) of SETD3 with His73 or selected histidine analog-replaced βA peptides in the presence of SAH and sinefungin (SFG), respectively. ITC titration experiments showed that the binding K_{D} values dropped from $0.7 \mu\text{M}$ for wild-type $\beta\text{A-His73}$ to 0.8 , 3.1 , 7.2 , and $44.4 \mu\text{M}$ for the $\beta\text{A-4-TriaA73}$, $\beta\text{A-4PyrAla73}$, $\beta\text{A-Orn73}$, and $\beta\text{A-3PyrAla73}$ peptides in the presence of SAH (Figure 5c and Figures S34–S41). Corresponding K_{D} values are 1.0 , 4.0 , 4.9 , 39.2 , and $48.5 \mu\text{M}$ in the presence of SFG (Figure 5d). The measured binding affinities in the presence of SAH are generally stronger than those in the presence of SFG, consistent with the previous report, and suggest the existence of steric tension between the bulkier SFG with the βA peptides at the active center.²²

2.5 | Co-crystal structural studies of SETD3 bound to analog βA peptides

To elucidate the molecular basis for substrate engagement by SETD3, we determined the crystal structures of SETD3- $\beta\text{A-Orn73-SAH}$ (PDB: 7W29) and SETD3- $\beta\text{A-4PyrAla73-SAH}$ (PDB: 7W28) ternary complexes at 2.9 \AA and 1.8 \AA resolution, respectively (Table S2). The overall engagement modes of histidine analogs with SETD3-SAH were similar to that of the native βA peptide. In the complex structure, the His73 analog and SAH are confined in the catalytic channel of SETD3 through a “head-to-head” mode (Figure 6a,b, close-up view). The $\beta\text{A-4PyrAla73}$ and $\beta\text{A-Orn73}$ peptides can be clearly traced and modeled according to the 2Fo–Fc omit map

(Figure 6c). Superimposition of the wild-type (PDB: 6MBJ) and the $\beta\text{A-Orn73}$ ternary complex structures revealed similar substrate engagement modes. We observed similar positioning ($\sim 0.6 \text{ \AA}$ shift) of the nitrogen atom of Orn73 terminal amine and the N^{τ} atom of histidine next to the sulfur atom of SAH at the active center, consistent with the decent methyltransferase activity measured for the $\beta\text{A-Orn73}$ substrate (Figure 6d). In the meantime, we observed clear twist of the C_{α} backbone of Orn73 as compared to His73 of wild type βA . This suggested steric tension likely caused by the bulkier size of the Orn73 side chain, thus accounting for the weaker K_{m} or K_{D} observed for the $\beta\text{A-Orn73}$ analog. Collectively, these results highlight exquisite substrate recognition mechanisms that may determine the substrate preference of SETD3. Structural alignment of the SETD3 wild-type $\beta\text{A-His73-SAH}$ (PDB: 6MBJ) and the $\beta\text{A-4PyrAla73-SAH}$ ternary complexes displayed the similar positioning of the N^{τ} atom of histidine and the nitrogen atom of 4PyrAla73 pyridine ring at the active center, consistent with the observed enzymatic activity (Figure 6e). Meanwhile, the bulkier size of the six-atom ring of 4PyrAla73 side chain may lead to fourfold decrease of the binding affinity in the presence of SAH (Figure 5). Further superimposition of SETD3- $\beta\text{A-4PyrAla73-SAH}$, SETD3- $\beta\text{A-His73-SAH}$, and SETD3- $\beta\text{A-His73-SFG}$ (PDB: 6JAT) revealed rotational adjustments of the rings at residue 73 to better fit the dimension of the catalytic pocket (Figure 6f). Collectively, our structural comparison analyses support conformational flexibility at the active center, which is responsible for the observed substrate diversity in this study.

2.6 | QM/MM MD and free energy simulations

Computer simulations were performed on $\beta\text{A-His73}$, $\beta\text{A-N}^{\tau}\text{-Me-His73}$, $\beta\text{A-4-TriaA73}$, $\beta\text{A-3PyrAla73}$, and $\beta\text{A-4PyrAla73}$ to provide additional information concerning the ability of SETD3 to catalyze methylation of these analogs as well as the energetic and structural origins of the activities. The crystal structure complex containing the

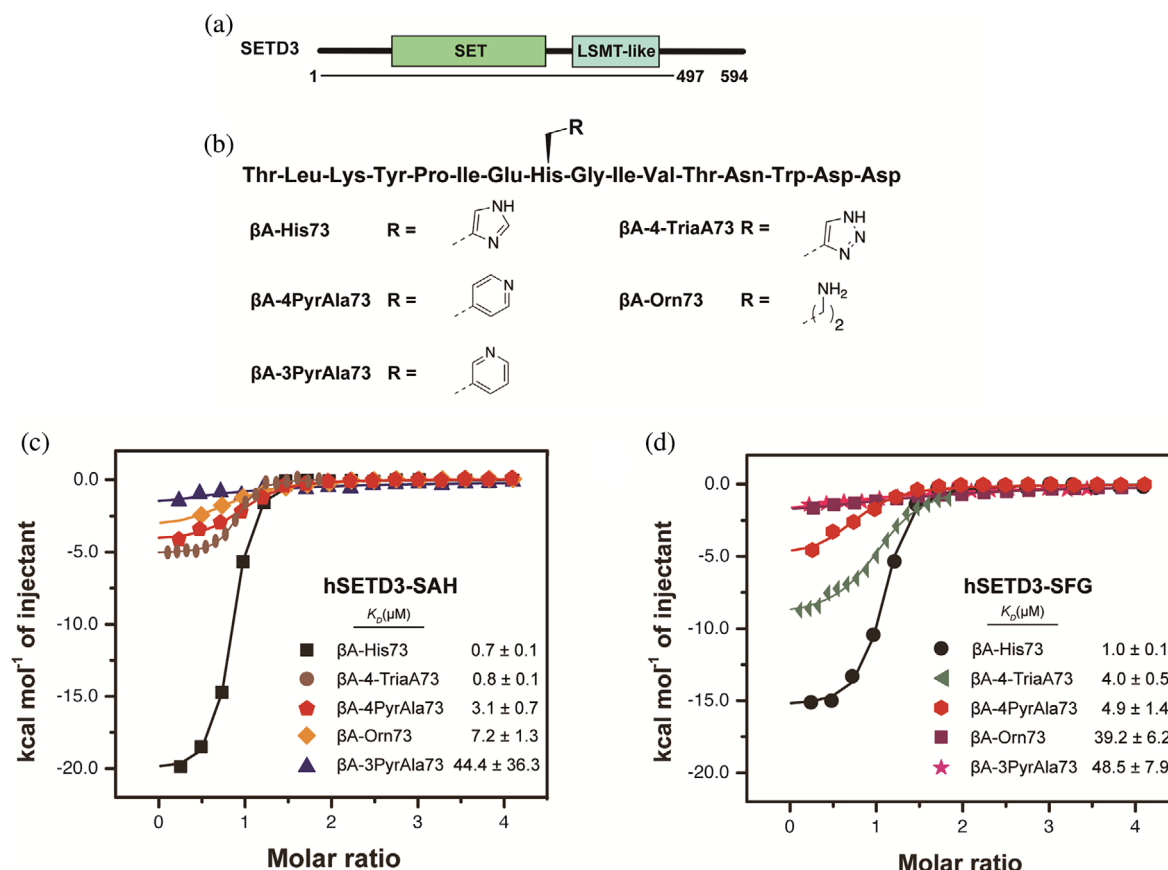


FIGURE 5 Binding studies of SETD3 with the β A peptide and its His73-replaced analogs. (a) Domain architecture of human SETD3. Underlined region is the expression frame of SETD3 for binding study. (b) The sequence and functional group information of peptides used for titration and crystallization. (c,d) ITC fitting curves of SETD3₁₋₄₉₇ titrated with wild-type β A peptide and analogs mentioned above in the presence of SAH or SFG

β A-4PyrAla73 peptide obtained in this work was used to build the models (see Section 4). The free energy profiles for methylation of β A-His73 and its mimics are plotted in Figure 7. As can be seen from Figure 7, the β A-His73 and β A-4-TriaA73 substrates have the lowest free energy barrier (15.4 and 17.4 kcal mol⁻¹, respectively). The results are consistent with the kinetics data in Table 1 showing that SETD3 is the most active on β A-His73 and β A-4-TriaA73 with the two highest k_{cat} values. For β A-N^π-Me-His73, β A-3PyrAla73, and β A-4PyrAla73, the free energy barriers are relatively higher, and these results are also consistent with the lower k_{cat} values observed for these analogs.

The average structures of the reactive state prior to the methyl transfer are given in Figure 8; other structural information obtained from the simulations are given in Figures S42–S47. Figure 8a shows that the structure for β A-His73 is quite close to the one obtained earlier based on a different crystal structure. For instance, there is a hydrogen bond between N^π-H and Asn255, which stabilizes an orientation of the imidazole ring similar to that

in the crystal structures of the product complex.^{20–23} It is of interest to notice that this hydrogen bond involving Asn255 also exists in the β A-4-TriaA73 complex (Figure 8b). The existence of this hydrogen bond is expected to play an important role in stabilizing the configuration of the 4-TriaA73 ring observed in the reactive state. The target N^π seems to be better positioned to accept the methyl group from SAM at such configuration (Figure 8b), and this may lead to a higher activity of SETD3 on β A-4-TriaA73 as observed experimentally. Consistent with this suggestion, previous experimental^{20,21} and computational studies²³ on β A-His73 have shown that the k_{cat} ($k_{\text{cat}}/K_{\text{m}}$) value decreased and the free energy barrier increased as a result of the Asn255Ala mutation, which removed the hydrogen bond involving Asn255. Figure 8c,d show that the rings of 3PyrAla73 and 4PyrAla73 underwent some rotations relative to those observed for β A-His73 and β A-4-TriaA73 with $\chi(\text{N}^{\pi}/\text{C}_{\delta 1} - \text{C}_{\beta} - \text{C}_{\gamma} - \text{C}_{\alpha})$ increasing about 40–70°. The alignments of the transferable methyl group on SAM with the lone-pair electron on N seem not as good as those

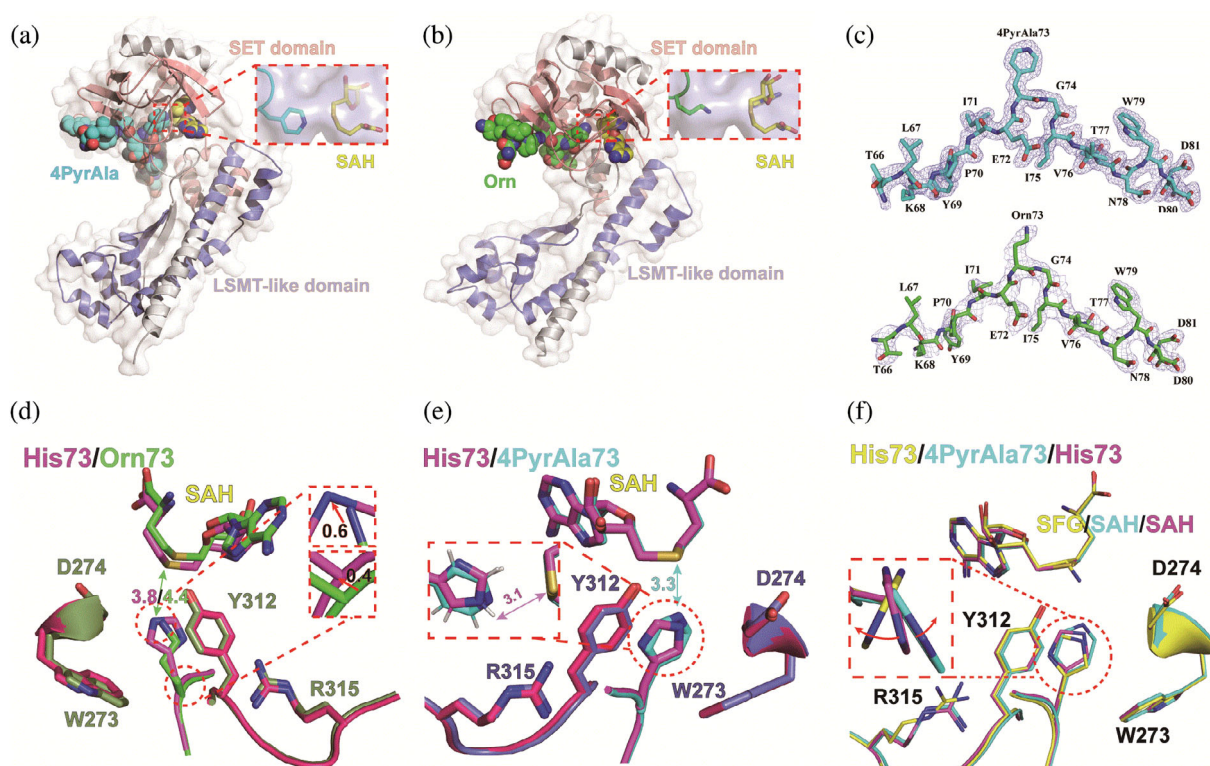


FIGURE 6 Structural characterization of SETD3 bound to histidine analog β A peptides. (a,b) Overall structures of SETD3 bound to β A-4PyrAla73 or β A-Orn73 peptide and SAH. The SET and LSMT-like domains of SETD3 are color-coded as indicated. SETD3 is shown in semitransparent surface view. 4PyrAla (cyan) or Orn (green) replaced in the β A peptides and SAH (yellow) are depicted as spheres, respectively. Close-up views, positioning of SAH and the methyl acceptor residues inside the catalytic channel. (c) $2F_o - F_c$ omit map of β A-4PyrAla73 and β A-Orn73 peptides contoured at 1.0σ level. (d,e) Interaction details of peptidyl substrates inserted into the active center of SETD3. His73 (red), Orn73 (green), and 4PyrAla73 (cyan) are shown as sticks, and distances between indicated atoms are labeled in the unit of angstrom with coded color. Functional groups of Orn73 and His73 are also depicted as color-coded meshes in close-up view of panel d. Key residues of SETD3 are depicted as green (Orn73) and blue (4PyrAla73) sticks. (f) Superimposition of SETD3 in complex with β A-4PyrAla73 (cyan) and β A-His73 in the presence of SAH (red) or SFG (yellow)

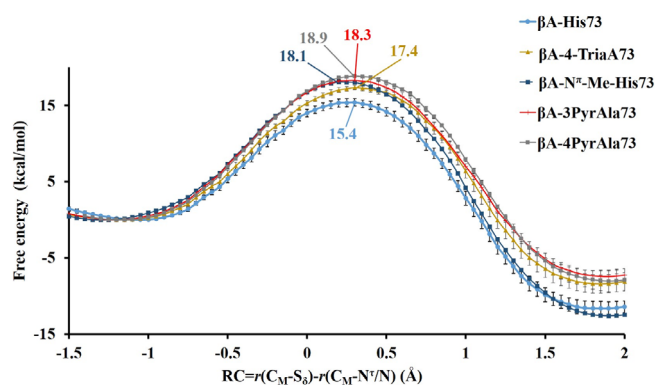


FIGURE 7 Free energy (PMF) profiles for the methyl transfer from SAM to the target N^ϵ/N for β A-His73, β A- N^ϵ -Me-His73, β A-4-TriaA73, β A-3PyrAla73, and β A-4PyrAla73, respectively, as a function of the reaction coordinate [$R = r(C_M - S_\delta) - r(C_M - N^\epsilon/N)$] obtained from the QM/MM free energy simulations

observed for β A-His73 and β A-4-TriaA73, and this may be related to the observations that SETD3 is less active on either of these two analogs (Table 1).

3 | CONCLUSION

Understanding protein PTMs is of central importance to structure and function of proteins, most notably established for histone proteins and their regulation of eukaryotic transcription.^{36–38} Histidine is a subject of several types of PTMs, including N^π - and N^τ -methylation,^{20,21,39} N^π - and N^τ -phosphorylation,^{40,41} and C_β -hydroxylation,^{42,43} most of them being only recently identified and characterized. To advance basic molecular understanding of histidine PTMs, it is essential to explore whether simplest histidine mimics are tolerated and modified by enzymes that install PTMs on histidine residues in proteins. The amber suppression method enabled incorporation of histidine mimics into proteins; however, it is limited to only few selected histidine analogs.^{44,45} While new chemical tools that rely on click-based phosphohistidine have enabled deeper biomolecular understanding of histone phosphorylation in the context of protein science,^{46–48} such and related tools for histidine methylation are currently lacking, leading to limited

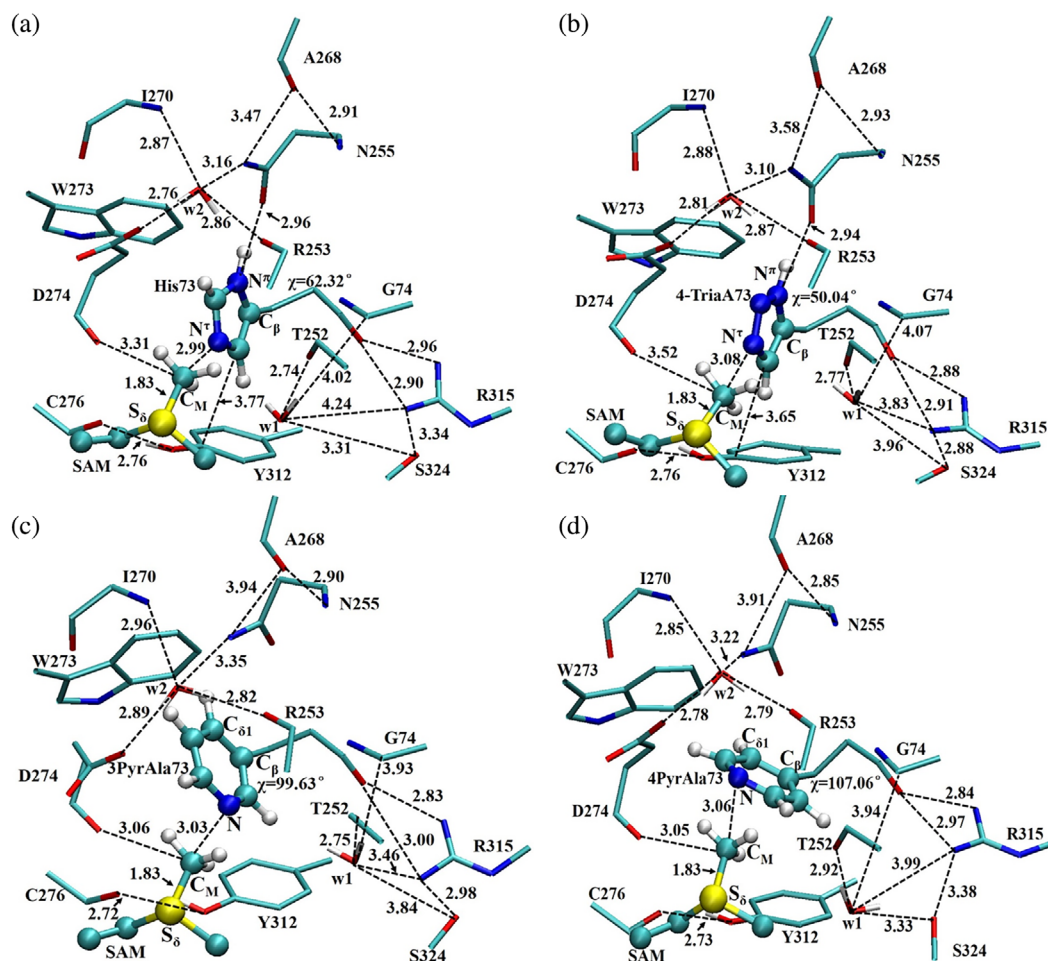


FIGURE 8 The average active-site structures of the reactive state obtained from QM/MM MD simulations. (a) β A-His73. (b) β A-4-TriaA73. (c) β A-3PyrAla73. (d) β A-4PyrAla73. The average structure for β A- N^π -Me-His73 and other structural information (e.g., those near transition state) are given in the Supporting Information

understanding of biologically important histidine methylation. To develop new tool compounds and deepen fundamental understanding of enzymatic histidine methylation, we have here for the first time explored a large panel of histidine mimics as potential substrates for methyltransferase SETD3, establishing its substrate specificity and biocatalytic potential. Our coordinated synthetic, enzymatic, biostructural, and computational studies provide strong evidence that human SETD3 has broader substrate specificity beyond histidine. Among the unnatural amino acids in our panel, triazol-4-yl-alanine and 4-pyridylalanine were observed as excellent SETD3 substrates, whereas N^π -methylhistidine, 3-pyridylalanine, and Orn were good, but comparatively poorer substrates. All five histidine analogs, however, display superior substrate efficiency relative to lysine and methionine, two natural amino acids that were recently identified as poor SETD3 substrates when incorporated into actin peptide and protein.^{26,27} Structural analyses of the ternary complexes suggest that SETD3 is a methyl

acceptor geometry-sensitive histidine methyltransferase because of its “head-to-head” engagement mode at the catalytic center. The substrate specificity of SETD3 is largely affected by the size compatibility between the acceptor group and the methyl donor SAM. Quantum mechanics/molecular mechanics molecular dynamics and free energy simulations further supported our experimental findings by revealing that some of these mimics could undergo methylation, and the efficiency of the methylation seems to correlate with the ability of the analogs to form the near attack conformations at the active site. Our work, together with recent studies on lysine and methionine methylation, demonstrates that SETD3’s unique ability to catalyze methylation of histidine residues can be extended to efficient methylation of its simple mimics. More generally, this work shows that a combination of state-of-the-art experimental and computational approaches enables investigations on enzymatic catalysis with an unprecedented level of molecular detail.

4 | METHODS

4.1 | SETD3 expression and purification

The recombinant human SETD3 fused to an N-terminal His₆-tag was produced and purified by a slightly modified procedure described by Kwiatkowski et al.¹⁴ Briefly, the enzyme was expressed in *Escherichia coli* BL21(DE3) at 13°C overnight in the presence of 0.3 mM IPTG. The recombinant protein was purified with HisTrap FF column (5 ml) and eluted in 20 ml of 50 mM HEPES pH 7.5, 400 mM NaCl, 10 mM KCl, 300 mM imidazole, and 1 mM DTT. The elution buffer was exchanged by sequential dialysis of the enzyme preparation against 500 ml of dialysis buffer (20 mM Tris-HCl pH 7.5, 200 mM NaCl, 1 mM DTT, and 6% sucrose) overnight at 4°C and then twice against 500 ml of the buffer for 3 hr at room temperature (RT). The enzyme purity was verified by SDS-PAGE (>97%). The purified enzyme was aliquoted and stored at -70°C.

4.2 | Synthesis and purification of β A peptides

All β A peptides were chain assembled on Rink amide resin using microwave assisted SPPS on a Liberty Blue peptide synthesizer (CEM corporation, Matthews, NC). All amino acid couplings were carried out with the equivalent ratio of [5]:[5]:[7.5] of [Fmoc-protected amino acid]:[DIC]:[Oxyma Pure] at 75°C for 2 min or at 50°C for 4 min for histidine, whereas histidine analogs were coupled at 50°C for 10 min. Peptides proceeded to standard cleavage from resin using 0.5% TIPS, 0.5% H₂O in conc. TFA. The Aza containing peptide was cleaved with 0.5% TIPS, 0.5% H₂O, 0.5% TES, and 0.5% thioanisole in conc. TFA. TFA was blown off using N₂ and the resultant residue suspended in cold Et₂O. After suspension it was subjected to centrifugation for 5 min at 5,000 rpm in an Eppendorf 5804R centrifuge (Eppendorf, Hamburg, Germany) after which the supernatant was decanted into the waste. The remaining white to yellow solid was washed twice by cold Et₂O and subjected to centrifugation after which the crude peptide was dissolved in a mixture of ACN in H₂O and purified using preparative reverse-phase HPLC (RP-HPLC) using a gradient of buffer A and buffer B from 20% B to 70% over 40 min at 4 ml/min using a Gemini 10 μ m NX-C18 110Å LC column (Phenomenex, Torrance, CA). Analytical RP-HPLC was carried out on a Gemini 5 μ m C18 110Å LC column (Phenomenex) at a flow rate of 1 mL/min. Analytical injections were monitored at 215 nm.

4.3 | General strategy for the on-resin generation of triazolylalanines

The click reagent (NaN₃ or TMS-acetylene, 45 eq.) was dissolved in 300 μ l MQ and then added to the β A peptide resin under argon atmosphere, followed by short mixing on vortex. CuSO₄ (6 eq.) was then dissolved in 200 μ l MQ and mixed with BTTP (2.6 eq.) followed by addition of sodium ascorbate (4 eq.) dissolved in 200 μ l MQ under argon atmosphere. This mixture was added to the peptide solution, followed by the addition of 40 μ l DIPEA, and was then reacted overnight at RT while shaking. The resin was then washed with DMF and DCM and subsequently TFA cleaved under standard conditions, diluted with 300 μ l ACN and directly purified on RP-HPLC using a gradient of buffer A and buffer B from 20% B to 70% over 40 min at 4 ml/min and subsequently lyophilized.

4.4 | Synthesis of C²-Me-His

The β A peptide was dissolved in H₂O:DMSO 9:1 (v/v) and heated to 70°C under argon atmosphere. A solution of sodium methanesulfinate (12 eq., 0.6 M) and TBHP (20 eq., 0.1 M) was added dropwise using a syringe pump (flowrate 100 μ l/min) and the reaction was left to stir overnight. The mixture was then diluted with ACN to a ratio of H₂O:ACN:DMSO 4.5:5:0.5 (v/v/v) and directly purified on RP-HPLC using a gradient of buffer A and buffer B from 20% B to 70% over 40 min at 4 ml/min and subsequently lyophilized.³²

4.5 | MALDI-TOF MS enzymatic assays

SETD3's enzymatic activity toward β A peptides was measured at different time points under standard conditions (1 μ M SETD3 enzyme, 10 μ M β A peptide, and 100 μ M SAM cosubstrate) in the reaction buffer at five different pH's: 3.5 (21.3 mM sodium citrate dihydrate, 78.7 mM citric acid, and 20 mM NaCl), 5.0 (57.7 mM sodium citrate dihydrate, 42.3 mM citric acid, and 20 mM NaCl), 7.2 (25 mM Tris-HCl and 20 mM NaCl), 9.0 (25 mM Tris-HCl and 20 mM NaCl), and 10.5 (20 mM glycine, 20 mM NaOH, and 50 mM NaCl). The reactions were carried out in a final volume of 50 μ l by incubation by shaking in a Thermomixer C (Eppendorf) at 750 rpm, at 37°C. Lys analogs and experiments carried out at pH 3.5 and 5.0 were incubated with elevated SETD3 concentrations as well (10 μ M SETD3, 10 μ M peptide, and 200 μ M SAM); these reactions were carried out in a final volume of 25 μ l. All reactions were quenched by the addition of 10% TFA

in MilliQ water (v/v), aliquoted and mixed 1:1 with α -Cyano-4-hydroxycinnamic acid (CHCCA) matrix dissolved in a mixture of H₂O and ACN (1:1, v/v), and loaded onto an MTP 384 polished steel target to be analyzed by a UltrafleXtreme-II tandem mass spectrometer (Bruker).

4.6 | MALDI-TOF MS kinetic assays

β A peptide kinetic evaluation was carried out with a MALDI-TOF MS assay under steady-state conditions at pH 9.0. β A peptides (0–125 μ M) and SAM (1 mM) were incubated and reactions were started by addition of SETD3 (100–400 nM, depending on the tested analog) in a final volume of 25 μ l. The reactions were carried out by incubation by shaking in a Thermomixer C (Eppendorf) at 750 rpm, at 37°C. Steady-state conditions were guaranteed by saturating concentrations of SAM (1 mM, $>5 \times K_m$ value). Reactions were quenched by the addition of 10% TFA in MQ after 20 min. All reactions were aliquoted, mixed 1:1 with CHCCA in a mixture of H₂O and ACN (1:1, v/v) and loaded onto an MTP 384 polished steel target to be analyzed by a MALDI-TOF MS. The amount of methylated peptide was calculated by integration of the product peak area and divided by the amount of total (methylated and unmethylated) peptide, taking in account all the ionic species. Kinetic values were extrapolated by fitting V_0 values and β A peptide concentrations to the Michealis–Menten equation using GraphPad Prism 5. Experiments were carried out in duplicate and final values are reported as value \pm SD.

4.7 | MALDI-TOF MS inhibition studies

β A peptides (10 μ M), SAM (100 μ M), and SETD3 (180 nM) were preincubated for 1 hr at 37°C at pH 9. Then, the β A-His73 peptide (sequence 66–81; 10 μ M) was added to the mixture to a final volume of 50 μ l and incubated for an additional 20 min at 37°C. The reactions were quenched by the addition of TFA 10% in MilliQ water, aliquoted and mixed 1:1 with CHCCA matrix dissolved in a mixture of H₂O and ACN (1:1, v/v), and loaded onto an MTP 384 polished steel target to be analyzed. SETD3 residual activity was determined by calculating the relative integral of the methylated peptide to a control reaction in absence of potential inhibitory peptides. Experiments were carried out in duplicate.

4.8 | Isothermal titration calorimetry

The titration was performed using the MicroCal PEAQ-ITC instrument (Malvern Instrument) at 25°C. Before

ITC titration, SETD3 was incubated with SAH or SFG in a molar ratio of 1:10 for 1 hr in buffer 20 mM Tris–HCl, pH 8.0 and 150 mM NaCl. Each ITC titration consisted of 17 successive injections. Usually, peptides at 0.5–1 mM were titrated into the complex of SETD3 and SAH or SFG at 0.05 mM. The resultant ITC curves were analyzed with Origin 7.0 (OriginLab) using the “One Set of Binding Sites” fitting model. Protein concentrations were measured based on the UV absorption at 280 nm.

4.9 | Crystallization, data collection, and structural determination

Crystallization was performed via the sitting drop vapor diffusion method at 16°C by mixing equal volume (0.2–1 μ l) of protein with reservoir solution. SETD3_{1–497} was premixed with SAH in a 1:10 M ratio in buffer containing 20 mM Tris–HCl, pH 8.0, and 150 mM NaCl. The protein sample was prepared by mixing SETD3_{1–497}–SAH complex with peptides in a molar ratio of 1:3 overnight at 4°C. The crystal of SETD3_{1–497}– β A-4PyrAla73–SAH was grown in a reservoir solution containing 30% (w/v) PEG4000, 0.1 M Tris–HCl, pH 8.5, and 0.2 M Li₂SO₄. The reservoir solution of SETD3_{1–497}– β A-Orn73–SAH was 20% (w/v) PEG6000, 0.1 M Bicine–NaOH, pH 9.0. The co-crystals were briefly soaked in cryoprotectant, composed of reservoir solution supplemented with 10% glycerol, and then flash-frozen in liquid nitrogen for data collection. Diffraction data of SETD3_{1–497}– β A-Orn73–SAH was collected at beamline BL17U1 at Shanghai Synchrotron Radiation Facility at 0.9792 Å. And the diffraction data set of SETD3_{1–497}– β A-4PyrAla73–SAH was collected at beamline BL19U2 at 0.9788 Å. Diffraction images were indexed, integrated, and merged using the HKL2000 software.⁴⁹ The structures were solved by molecular replacement using Molrep⁵⁰ from the CCP4 suite with SETD3– β A-His73–SAH (PDB ID: 6MBJ) as the search model. Refinement and model building was performed with PHENIX⁵¹ and COOT,⁵² respectively. The data collection and structural refinement statistics are summarized in Table S2.

4.10 | Computational analysis

QM/MM MD and free energy (PMF) simulations were performed to study the structural properties and dynamics of the reactive state of the enzyme–substrate complex for methylation and to calculate the free energy profile for the methyl transfer from SAM to N¹/N of the target His73 or analog (β A-His73, β A-N ^{π} -Me-His73, β A-4-TriaA73, β A-3PyrAla73, or β A-4PyrAla73) in wild-type SETD3 using the CHARMM program.⁵³ The –CH₂–CH₂–

$S^+(\text{Me})\text{-CH}_2\text{-}$ part of SAM and the analog side-chain were treated by QM and the rest of the system by MM. The link-atom approach⁵⁴ was applied to separate the QM and MM regions. A modified TIP3P water model⁵⁵ was employed for the solvent, and the stochastic boundary molecular dynamics method⁵⁶ was used for the QM/MM MD and free energy simulations. The system was separated into a reaction zone and a reservoir region, and the reaction zone was further divided into a reaction region and a buffer region. The reaction region was a sphere with radius r of 20 Å, and the buffer region extended over $20 \text{ \AA} \leq r \leq 22 \text{ \AA}$. The reference center for partitioning the system was chosen to be the N^τ atom of the His residue. The resulting systems contained around 5,700 atoms, including about 500 water molecules. The DFTB3 method^{57–60} implemented in CHARMM was used for the QM atoms and the all-hydrogen CHARMM potential function (PARAM27)⁶¹ was used for the MM atoms. The initial structures for the entire stochastic boundary systems were optimized using the steepest descent and adopted-basis Newton–Raphson methods. The systems were gradually heated from 50.0 to 298.15 K in 50 ps. A 1-fs time step was used for integration of the equation of motion, and the coordinates were saved every 50 fs for analyses; 5 ns QM/MM MD simulations were carried out for each of the structures of the reactive state and the distribution maps of $r(\text{C}_M\text{-N}^\tau)$ and θ were generated in each case; here, θ is defined as the angle between the direction of the $\text{C}_M\text{-S}_\delta$ bond and the direction of the electron lone pair on N^τ/N . Classical MD simulations (30 ns) with CHARMM force field were also performed to confirm the structure and stability of the reactive state for methylation. To make sure that our computational approaches can re-produce the experimental structures, the QM/MM MD simulations were also performed for the product complex based on the crystal structures. It was found that the experimental structures could be well re-produced using our computational approaches.

The structures of the reactive state for methylation were generated based on the crystal structure of the SETD3 complex containing the $\beta\text{A-4PyrAla73}$ peptide obtained in this work. SAH in the crystal structure was changed to SAM manually and the $\beta\text{A-4PyrAla73}$ peptide was changed to $\beta\text{A-His73}$, $\beta\text{A-N}^\tau\text{-Me-His73}$, $\beta\text{A-4-TriaA73}$, or $\beta\text{A-3PyrAla73}$ to study the methylation process involving each of these peptides; for $\beta\text{A-4PyrAla73}$, the coordinates from the crystal structure were used directly. The imidazole ring of His73 was generated as the $N^\tau\text{-H}$ tautomer with N^τ unprotonated and N^π protonated before the simulations were performed; the imidazole ring rotated around the $\text{C}_\beta\text{-C}_\gamma$ bond during the QM/MM MD simulations, leading to the orientation similar to that in the product complex.^{20,21} The umbrella

sampling method⁶² implemented in the CHARMM program along with the Weighted Histogram Analysis Method⁶³ was applied to determine the change of the free energy (potential of mean force) as a function of the reaction coordinate for the methyl transfer from SAM to His73/analog in SETD3. The reaction coordinate was defined as a linear combination of $r(\text{C}_M - N^\tau/N)$ and $r(\text{C}_M - S_\delta)$ [$R = r(\text{C}_M - S_\delta) - r(\text{C}_M - N^\tau/N)$]. For the methyl transfer process, 25 windows were used, and for each window 100 ps production runs were performed after 50 ps equilibration. The force constants of the harmonic biasing potentials used in the PMF simulations were 50–400 kcal mol⁻¹ Å⁻². In each case, five independent PMF simulations were performed. The free energies (PMFs) and statistical errors were taken as the average values and standard deviations from the five runs, respectively. High-level ab initio calculations (i.e., B3LYP/6-31G**) are too time-consuming for generating free energy profiles of enzyme-catalyzed reactions. The semi-empirical approach based on DFTB3 has been used previously on a number of systems, and the results seem to be quite reasonable for the estimate of the relative free energy barriers along a given reaction coordinate involving wild-type and mutants.^{59,60} It should be pointed out that the bond breaking and making events studied in this work involve simple and similar S_N2 methyl transfer processes so that much of the errors for the methyl transfers in His73 and different analogs are presumably similar and canceled out when the relative free energy profiles are compared.

4.11 | Data deposition

Coordinates of SETD3- $\beta\text{A-4PyrAla73}$ and SETD3- $\beta\text{A-Orn73}$ have been deposited into the Protein Data Bank under accession codes 7W28 and 7W29, respectively.

ACKNOWLEDGEMENTS

This research was supported by the European Research Council (ERC Starting Grant, ChemEpigen-715691 to Jasmin Mecinović), an Opus-14 grant from the National Science Centre, Poland (2017/27/B/NZ1/00161 to Jakub Drozak), National Natural Science Foundation of China (22177064 to Ping Qian), the Natural Science Foundation of Shandong Province (ZR2021MB050 to Ping Qian), National Natural Science Foundation of China (31725014 to Haitao Li) and National Key Research Development Program of China (2020YFA0803300 to Haitao Li).

CONFLICT OF INTEREST

The authors have declared no conflicts of interest for this article.

AUTHOR CONTRIBUTIONS

Jordi C. J. Hintzen: Investigation (supporting); methodology (equal); writing – original draft (equal). **Huida Ma:** Investigation (supporting); methodology (equal). **Hao Deng:** Investigation (supporting); methodology (equal). **Apolonia Witecka:** Methodology (supporting). **Steffen B. Andersen:** Methodology (supporting). **Jakub Drozak:** Funding acquisition (equal); methodology (supporting); supervision (supporting). **Hong Guo:** Investigation (supporting); methodology (equal); supervision (supporting); writing – original draft (equal). **Ping Qian:** Funding acquisition (equal); investigation (lead); methodology (equal); supervision (equal); writing – original draft (equal). **Haitao Li:** Funding acquisition (equal); investigation (lead); methodology (lead); supervision (equal); writing – original draft (equal). **Jasmin Mecinović:** Funding acquisition (lead); investigation (lead); methodology (lead); supervision (equal); writing – original draft (lead).

ORCID

Jasmin Mecinović  <https://orcid.org/0000-0002-5559-3822>

REFERENCES

- dos Remedios CG, Chhabra D, Kekic M, et al. Actin binding proteins: regulation of cytoskeletal microfilaments. *Physiol Rev.* 2003;83:433–473.
- Dominguez R, Holmes KC. Actin structure and function. *Annu Rev Biophys.* 2011;40:169–186.
- Pollard TD, Cooper JA. Actin, a central player in cell shape and movement. *Science.* 2009;326:1208–1212.
- Campellone KG, Welch MD. A nucleator arms race: cellular control of Actin assembly. *Nat Rev Mol Cell Biol.* 2010;11:237–251.
- Perrin BJ, Ervasti JM. The Actin gene family: function follows isoform. *Cytoskeleton.* 2010;67:630–634.
- Letterrier C, Dubey P, Roy S. The nano-architecture of the axonal cytoskeleton. *Nat Rev Neurosci.* 2017;18:713–726.
- Pieters BJGE, van Eldijk MB, Noltje RJM, Mecinović J. Natural supramolecular protein assemblies. *Chem Soc Rev.* 2016;45:24–39.
- Lappalainen P. Actin-binding proteins: the long road to understanding the dynamic landscape of cellular Actin networks. *Mol Biol Cell.* 2016;27:2519–2522.
- Varland S, Vandekerckhove J, Drazic A. Actin post-translational modifications: The Cinderella of cytoskeletal control. *Trends Biochem Sci.* 2019;44:502–516.
- Terman JR, Kashina A. Post-translational modification and regulation of Actin. *Curr Opin Cell Biol.* 2013;25:30–38.
- Kabsch W, Mannherz HG, Suck D, Pai EF, Holmes KC. Atomic structure of the Actin: DNase I complex. *Nature.* 1990;347:37–44.
- Nyman T, Schüler H, Korenbaum E, Schutt CE, Karlsson R, Lindberg U. The role of MeH73 in Actin polymerization and ATP hydrolysis. *J Mol Biol.* 2002;317:577–589.
- Wilkinson AW, Diep J, Dai S, et al. SETD3 Is an Actin histidine methyltransferase that prevents primary dystocia. *Nature.* 2019;565:372–376.
- Kwiatkowski S, Seliga AK, Vertommen D, et al. SETD3 protein is the Actin-specific histidine N-methyltransferase. *Elife.* 2018;7:e37921.
- Witecka A, Kwiatkowski S, Ishikawa T, Drozak J. The structure, activity and function of the SETD3 protein histidine methyltransferase. *Life.* 2021;11:1040.
- Carlson SM, Gozani O. Nonhistone lysine methylation in the regulation of cancer pathways. *CSH Perspect Med.* 2016;6:a026435.
- Dillon SC, Zhang X, Trievel RC, Cheng X. The SET-domain protein superfamily: Protein lysine methyltransferases. *Genome Biol.* 2005;6:227.
- Eom GH, KimK-B KJH, Kim J-Y, et al. Histone methyltransferase SETD3 regulates muscle differentiation. *J Biol Chem.* 2011;286:34733–34742.
- Wagner EJ, Capenter PB. Understanding the language of Lys36 methylation at histone H3. *Nat Rev Mol Cell Biol.* 2012;13:115–126.
- Guo Q, Liao S, Kwiatkowski S, et al. Structural insights into SETD3-mediated histidine methylation on β -Actin. *Elife.* 2019;8:e43676.
- Dai S, Horton JR, Woodcock CB, et al. Structural basis for the target specificity of Actin histidine methyltransferase SETD3. *Nat Commun.* 2019;10:3541.
- Zheng Y, Zhang X, Li H. Molecular basis for histidine N3-specific methylation of Actin H73 by SETD3. *Cell Discov.* 2020;6:3.
- Deng H, Ma Y, Ren W-S, Vuong VQ, Qian P, Guo H. Structure and dynamics of the reactive state for histidine methylation process and catalytic mechanism of SETD3: Insights from quantum mechanics/molecular mechanics investigation. *ACS Catal.* 2020;10:13314–13322.
- Nair UB, Joel PB, Wan Q, Lowey S, Rould MA, Trybus KM. Crystal structures of monomeric Actin bound to cytochalasin D. *J Mol Biol.* 2008;384:848–864.
- Rould MA, Wan Q, Joel PB, Lowey S, Trybus KM. Crystal structures of expressed non-polymerizable monomeric Actin in the ADP and ATP states. *J Biol Chem.* 2006;281:31909–31919.
- Dai S, Holt MV, Horton JR, et al. Characterization of SETD3 methyltransferase mediated protein methionine methylation. *J Biol Chem.* 2020;295:10901–10910.
- Dai S, Horton JR, Wilkinson AW, Gozani O, Zhang X, Cheng X. An engineered variant of SETD3 methyltransferase alters target specificity from histidine to lysine methylation. *J Biol Chem.* 2020;295:2582–2589.
- Qian C, Zhou MM. SET domain protein lysine methyltransferases: Structure, specificity and catalysis. *Cell Mol Life Sci.* 2006;63:2755–2763.
- Bilgin N, Moesgaard L, Maas MN, et al. Importance of Ile71 in β -Actin on histidine methyltransferase SETD3 catalysis. *Org Biomol Chem.* 2022;20:1723–1730.
- Hintzen JJC, Moesgaard L, Kwiatkowski S, Drozak J, Kongsted J, Mecinović J. β -Actin peptide-based inhibitors of histidine methyltransferase SETD3. *ChemMedChem.* 2021;16:2695–2702.
- Siegl SJ, Vázquez A, Dzajak R, et al. Design and synthesis of aza-bicyclononene dienophiles for rapid fluorogenic ligations. *Chem A Eur J.* 2018;24:2426–2432.
- Noisier AFM, Johansson MJ, Knerr L, et al. Late-stage functionalization of histidine in unprotected peptides. *Angew Chem Int Ed Engl.* 2017;58:13264–13267.

33. Belle R, Al Temimi AHK, Kumar K, et al. Investigating D-lysine stereochemistry for epigenetic methylation, demethylation and recognition. *Chem Commun*. 2017;53:13264–13267.
34. Al Temimi AHK, Teeuwen RS, Tran V, et al. Importance of the main chain of lysine for histone lysine methyltransferase catalysis. *Org Biomol Chem*. 2019;17:5693–5697.
35. Konášová R, Dyrtrtová JJ, Kašička V. Determination of acid dissociation constants of triazole fungicides by pressure assisted capillary electrophoresis. *J Chromatogr A*. 2015;1408:243–249.
36. Walsh CT. *Posttranslational modification of proteins: Expanding nature's inventory*. Englewood, CO: Roberts and Company Publishers, 2006.
37. Müller MM, Muir TW. Histones: at the crossroads of peptide and protein chemistry. *Chem Rev*. 2015;115:2296–2349.
38. Strahl BD, Allis CD. The language of covalent histone modifications. *Nature*. 2000;403:41–45.
39. Davydova E, Shimazu T, Schuhmacher MK, et al. The methyltransferase METTL9 mediates pervasive 1-methylhistidine modification in mammalian proteomes. *Nat Commun*. 2021;12:891.
40. Potel CM, Lin M-H, Heck AJ, Lemeer S. Widespread bacterial protein histidine phosphorylation revealed by mass spectrometry-based proteomics. *Nat Methods*. 2018;15:187–190.
41. Fuhs SR, Hunter T. pHisphorylation: The emergence of histidine phosphorylation as a reversible regulatory modification. *Curr Opin Cell Biol*. 2017;45:8–16.
42. Ge W, Wolf A, Feng T, et al. Oxygenase-catalyzed ribosome hydroxylation occurs in prokaryotes and humans. *Nat Chem Biol*. 2012;8:960–962.
43. Bundred JR, Hendrix E, Coleman ML. The emergin roles of ribosomal histidine hydroxylases in cell biology, physiology and disease. *Cell Mol Life Sci*. 2018;75:4093–4105.
44. Sharma V, Wang Y-S, Liu WR. Probing the catalytic charge-relay system in alanine racemase with genetically encoded histidine mimetics. *ACS Chem Biol*. 2016;11:3305–3309.
45. Xiao H, Peters FB, Yang P-Y, Reed S, Chitturulu JR, Schultz PG. Genetic incorporation of histidine derivatives using an engineered pyrrolyl-tRNA synthetase. *ACS Chem Biol*. 2014;9:1092–1096.
46. Kalagiri R, Stanfield RL, Meisenheider J, et al. Structural basis for differential recognition of phosphohistidine-containing peptides by 1-pHis and 3-pHis monoclonal antibodies. *Proc Natl Acad Sci USA*. 2021;118:e2010644118.
47. Kee J-M, Villani B, Carpenter LR, Muir TW. Development of stable phosphohistidine analogues. *J Am Chem Soc*. 2010;132:14327–14329.
48. Makwana MV, Muimo R, Jackson RFW. Advances in development of new tools for the study of phosphohistidine. *Lab Invest*. 2018;98:291–303.
49. Otwinowski Z, Minor W. Processing of X-ray diffraction data collected in oscillation mode. *Methods Enzymol*. 1997;276:307–326.
50. Vagin A, Teplyakov A. Molecular replacement with MOLREP. *Acta Crystallogr D*. 2010;66:22–25.
51. Adams PD, Afonine PV, Bunkóczi G, et al. PHENIX: A comprehensive Python-based system for macromolecular structure solution. *Acta Crystallogr D*. 2010;66:213–221.
52. Emsley P, Cowtan K. Coot: Model-building tools for molecular graphics. *Acta Cryst D*. 2004;60:2126–2132.
53. Brooks BR, Bruccoleri RE, Olafson BD, States DJ, Swaminathan S, Karplus M. CHARMM—a program for macromolecular energy, minimization, and dynamics calculations. *J Comput Chem*. 1983;4:187–217.
54. Field MJ, Bash PA, Karplus MA. Combined quantum-mechanical and molecular mechanical potential for molecular-dynamics simulations. *J Comput Chem*. 1990;11:700–733.
55. Jorgensen WL, Chandrasekhar J, Madura JD, Impey RW, Klein ML. Comparison of simple potential functions for simulating liquid water. *J Chem Phys*. 1983;79:926–935.
56. Brooks CL, Brunger A, Karplus MA. Active-site dynamics in protein molecules—a stochastic boundary molecular-dynamics approach. *Biopolymers*. 1985;24:843–865.
57. Elstner M, Porezag D, Jungnickel G, et al. Self-consistent-charge density-functional tight-binding method for simulations of complex materials properties. *Phys Rev B*. 1998;58:7260–7268.
58. Cui Q, Elstner M, Kaxiras E, Frauenheim T, Karplus MA. QM/MM implementation of the self-consistent charge density functional tight binding (SCC-DFTB) method. *J Phys Chem B*. 2001;105:569–585.
59. Christensen AS, Kubar T, Cui Q, Elstner M. Semiempirical quantum mechanical methods for noncovalent interactions for chemical and biochemical applications. *Chem Rev*. 2016;116:5301–5337.
60. Lu X, Gaus M, Elstner M, Cui Q. Parametrization of DFTB3/3-OB for magnesium and zinc for chemical and biological applications. *J Phys Chem B*. 2015;119:1062–1082.
61. MacKerell AD, Bashford D, Bellott M, et al. All-atom empirical potential for molecular modeling and dynamics studies of proteins. *J Phys Chem B*. 1998;102:3586–3616.
62. Torrie GM, Valleau JP. Monte-Carlo free-energy estimates using non-Boltzmann sampling—application to subcritical Lennard-Jones fluid. *Chem Phys Lett*. 1974;28:578–581.
63. Kumar S, Bouzida D, Swendsen RH, Kollman PA, Rosenberg JM. The weighted histogram analysis method for free-energy calculations on biomolecules. *J Comput Chem*. 1992;13:1011–1021.

SUPPORTING INFORMATION

Additional supporting information may be found in the online version of the article at the publisher's website.

How to cite this article: Hintzen JCJ, Ma H, Deng H, Witecka A, Andersen SB, Drozak J, et al. Histidine methyltransferase SETD3 methylates structurally diverse histidine mimics in actin. *Protein Science*. 2022;31(5):e4305. <https://doi.org/10.1002/pro.4305>